



Manuscript prepared for Atmos. Chem. Phys.
with version 2015/09/17 7.94 Copernicus papers of the L^AT_EX class copernicus.cls.
Date: 28 January 2016

Observing local turbulence and anisotropy during the afternoon transition with an unmanned aerial system - a case study

A. Lampert¹, F. Pätzold¹, L. Lobitz¹, S. Martin², G. Lohmann³, G. Canut⁴,
D. Legain⁴, and J. Bange⁵

¹Institute of Flight Guidance, TU Braunschweig, Germany

²Institute of Climatology and Environmental Meteorology, TU Braunschweig, Germany

³Energy Meteorology Group, Institute of Physics, Oldenburg University, Germany

⁴CNRM-GAME, UMR3589, Météo-France and CNRS, Toulouse, France

⁵Eberhard Karls University Tübingen, Germany

Correspondence to: Astrid Lampert (Astrid.Lampert@tu-bs.de)

Abstract. The article analyses airborne observations of turbulence in vertical and horizontal direction during the afternoon transition from turbulently mixed to stably stratified atmospheric conditions. The data were obtained during four flights at 14:30, 16:30, 18:30 and 20:30 UTC with the Meteorological Mini Aerial Vehicle M²AV during the BLLAST field experiment in summer 2011, which corresponds to 16:30, 18:30, 20:30 and 22:30 local time. Sunset was at 19:42 UTC. The anisotropy ratio defined here as the ratio of the variance of horizontal to vertical wind speed changes during the afternoon transition from a mean value about 1 to a mean value around 2 about one hour before sunset and then to a mean value around 8 at around one hour after sunset. The strongly enhanced horizontal wind speed variance during stable conditions in the lowermost 400 m is explained by a nocturnal Low-Level Jet (LLJ) as a source for turbulence in the horizontal direction. The gradient Richardson number indicates the generation of turbulence for the first and last flight only, where turbulence was created by thermal convection during the first flight, and by wind shear during the last flight. The development and small-scale inhomogeneous distribution of an LLJ was further analysed with frequent radiosonde and wind profiler observations.

15 1 Introduction

The afternoon-evening transition (AT) of the atmospheric boundary layer (ABL) describes the processes converting a turbulently mixed ABL into a stably stratified nocturnal ABL. The afternoon transition is defined differently in the literature, depending on the observational techniques and available data sets. Lothon et al. (2014) use the definition of Nadeau et al. (2011) for the BLLAST (Boundary-Layer Late Afternoon and Sunset Turbulence) experiment, according to which the AT begins when the surface sensible heat flux starts to decrease, and ends when the surface sensible



heat flux becomes negative, corresponding to the time before sunset. The whole evolution takes typically about 160 min during summer (Busse and Knupp, 2012). The transition usually includes several consecutive changes of near surface parameters: a decrease of the vertical and horizontal
25 wind variance, temperature, thermal fluctuations, and wind speed, as well as an increase of the mixing ratio, and finally the formation of a temperature inversion, e.g. Busse and Knupp (2012); Bonin et al. (2013). During the afternoon transition, the decay of turbulent kinetic energy per mass unit, in the following simply called TKE, is described as two consecutive distinct phases: first the TKE decreases at the upper part of the ABL, as the surface heating by solar radiation, being the source of
30 thermal mixing, gradually decreases. Then TKE is reduced throughout the entire ABL, while local anisotropy is highest at the top of the ABL (Darbieu et al., 2015). Bonin et al. (2013) estimated profiles of sensible and latent heat fluxes based on the temporal development of temperature and humidity profiles obtained with unmanned aerial systems. For two particular days, they determined an average negative sensible heat flux and a positive latent heat flux during the AT in Oklahoma in
35 October 2010 and February 2011.

Generally, the assumption of isotropic turbulence distribution in the atmosphere is a simplification which is not necessarily fulfilled (e.g., Lovejoy et al., 2011). During unstable stratification, turbulence is mainly generated by buoyancy induced by heating of the Earth's surface, therefore the variance in the vertical wind component is stronger than in the horizontal wind components. During
40 stable stratification, turbulence is mainly generated by vertical wind shear, leading to larger variance in the horizontal than in the vertical wind components (e.g., Mauritsen and Svensson, 2007). Therefore, as the atmospheric conditions change from turbulently mixed to stably stratified during the AT, turbulence anisotropy changes (Darbieu et al., 2015).

This article provides a case study of a particular cloud free day with low near ground wind speed, and
45 a typical development of the afternoon transition based on data sets collected during BLLAST, with a focus on turbulence measurements obtained by the Meteorological Mini Aerial Vehicle (M^2AV). The analysis of turbulence development is continued for the time after sunset, which strictly speaking is not part of the AT any more, but which is of interest due to large changes in turbulence parameters. Besides a general analysis of the ABL transition, the authors compare the magnitude of turbulent
50 kinetic energy during the transition from turbulently mixed to stably stratified conditions. In comparison with the case study of Darbieu et al. (2015), who analysed the turbulence development for another day, 20 June 2011, during the same field experiment, this case study provides turbulence observations at a higher temporal resolution, and includes an analysis of turbulence after sunset. However, in contrast to the other case study, turbulence properties are only available at a limited
55 number of altitudes, not throughout the whole ABL. The turbulence observations after sunset are linked to the evolution of a Low-Level Jet with data sets obtained by frequent radiosonde and radar wind profiler.



2 Background, experimental setup, data processing

2.1 Field site and instrumentation

60 The Boundary Layer Late Afternoon and Sunset Turbulence (BLLAST) experiment was conducted
in summer 2011 in southern France, about 10 km North of the Pyrenee mountains (Lothon et al.,
2014). It was dedicated to investigating the AT. The aim was to gain a deeper understanding of the
ABL transition from a turbulently mixed boundary layer to the nocturnal stably stratified atmosphere
by applying multi-scale complementary observation techniques. Three different sites spanning a tri-
65 angle with about 3–4 km sides were equipped with various in situ and remote sensing instruments
for comprehensive observations of the ABL. Additionally, different unmanned aerial vehicles were
operated within a radius of 2 km around one of the sites. Manned aircraft probed the atmosphere on
a larger scale with a radius of 20 km around the ground-based sites (Lothon et al., 2014).

The analyses focus on a case study for 2 July 2011. The analysed data sets include two ultra high fre-
70 quency (UHF) wind profilers at two locations about 4 km apart, which allow to determine the bound-
ary layer altitude (Angevine et al., 1994), hourly radiosonde ascents by the "frequent radiosonde"
technique (Legain et al., 2013), and data from the M²AV. The UHF data have a vertical resolution
of 75 m and were averaged over 30 min. The frequent radiosonde consists of a conventional Vaisala
receiver and a global positioning system (GPS) radiosonde recording pressure, wind, humidity and
75 temperature, that is tied to a couple of inflated balloons. The principle of the sounding system is to
permit a first balloon to detach from the rawinsonde at a predetermined altitude, allowing for the
rawinsonde to slowly descend with the second balloon as a parachute to perform a second sounding
near the landing location. The retrieved radiosonde is checked, and used for the next sounding. Ra-
diosonde times refer to the launching time in this manuscript. The locations for the different systems
80 and the flight tracks are shown in Fig. 1. Frequent radiosondes were launched about 1 km East of
the UHF radar site 2, and landed depending on wind direction and wind speed up to about 10 km
downwind.

The M²AV is an unmanned aerial vehicle with a wing span of 2 m and a weight of 6 kg. It is started
and landed manually, and controlled during the mission by an autopilot system. For this case study,
85 ascents and descents were flown manually, and the race track pattern with straight horizontal legs
were flown with the autopilot. The M²AV is equipped with a miniaturized turbulence measurement
payload comprising a 5-hole probe for deriving the angle of attack and sideslip in the aerodynamic
coordinate system, which can then be converted to the 3D wind vector in the geodetic coordinate
system using precise information on position and attitude of the aircraft obtained by GPS and an
90 inertial measurement unit (IMU). The application of the method for unmanned aircraft is demon-
strated by van den Kroonenberg et al. (2008). Further, the payload comprises a slow and accurate as
well as a fast temperature sensor, and a capacitive humidity sensor (Martin et al., 2011). The M²AV
performance has been validated extensively against other airborne data sets (Spiess et al., 2007),



as well as in situ meteorological tower and remote sensing observations (Martin et al., 2011). The
95 system has been deployed for high resolution atmospheric profiling (Martin et al., 2011; Jonassen
et al., 2015) and for deriving turbulent parameters (van den Kroonenberg et al., 2012; Martin et al.,
2014; Martin and Bange, 2014) worldwide at various locations.

For this study, the M²AV performed vertical profiles, and followed race track patterns of about 1 km
length for deriving turbulent parameters of the 3D wind vector. The race track pattern consisted of
100 three legs at one altitude (300 m) oriented in East-West and West-East direction, then three legs at a
second altitude (250 m) and two legs at a third altitude (200 m). The same pattern was repeated three
times for each flight. The same flight track was employed during four distinct flights starting around
14:30 UTC (corresponding to 16:30 local time), 16:30, 18:30 and 20:30 UTC. A single flight lasted
approximately 40 min. Only Flight 2 was shorter due to a failure of the autopilot around 20 min af-
105 ter takeoff. The exact times for takeoff and landing are given in Table 1. During the last flight, the
altitudes for the race track pattern were reduced by 50 m in response to the lower ABL height.

2.2 M²AV data processing

The static air temperature was derived from a Pt1000 thermometer measuring the stagnation point
temperature by correcting the time lag effect and the total temperature effect as described in Stick-
110 ney et al. (1994) using individual coefficients for the M²AV. The dry potential temperature was then
calculated according to Stull (1988). The profiles of wind speed were averaged over intervals of
10 m altitude for an individual ascent or descent. The profiles of wind direction were additionally
smoothed using a spline function.

For investigating the turbulence anisotropy, the variance of wind speed for the wind components
115 perpendicular to the flight track, in horizontal direction v , and in vertical direction w (meteorologi-
cal coordinate system) is analysed. This approach has been used in the literature by e.g. Paluch and
Baumgardner (1989); Gultepe and Starr (1995); Meischner et al. (2001). Further, as the prevailing
wind direction was from North during the day, the horizontal wind component v corresponds to the
along-wind data, which has a higher coherence than the cross-wind component according to e.g.
120 Thebaud (2004). The variances of wind speed σ_v^2 and σ_w^2 were calculated by different methods:

- removing the mean value and a linear trend of the time series for the wind speed for each leg, e.g. Martin and Bange (2014).
- employing a high pass Butterworth filter of third order, with different cutoff frequencies tested.

The variance values derived with the linear detrending function are systematically higher. Visual
125 inspection of the time series of v and w revealed several cases with wave like slowly changing
structures (wavelength around 2 km) of relatively large amplitude compared to the fast fluctuations.
They have a high impact on the variance calculation. By the high pass filtering technique, these fea-
tures disappeared. In any case, the flight legs were not long enough for obtaining statistically relevant
information about wavelengths larger than the double of the flight leg. Therefore, a 0.01 Hz high pass



130 filtering was finally applied to eliminate an advective contribution to TKE, instead of removal of a linear trend from the wind components. In this case study, only turbulence data calculated with the second method are used.

Further, TKE is calculated for each flight leg defined as (Stull, 1988)

$$TKE = \frac{1}{2}(\langle (w)^2 \rangle + \langle (v)^2 \rangle + \langle (u)^2 \rangle) = \frac{1}{2}(\sigma_u^2 + \sigma_v^2 + \sigma_w^2). \quad (1)$$

135 Assuming isotropy in the horizontal direction, the component w' in parallel direction to the aircraft track can be replaced by v' . Then Eq. 1 results in

$$TKE = (\langle (v)^2 \rangle + \frac{1}{2} \langle (w)^2 \rangle) = (\sigma_v^2 + \frac{1}{2} \sigma_w^2). \quad (2)$$

Equation 2 was further used in this study. The anisotropy ratio was defined in this study as the ratio of the variance of the horizontal wind speed normal to the flight track versus the variance of the

140 vertical wind speed component:

$$A = \frac{\sigma_v^2}{\sigma_w^2} \quad (3)$$

This is different from other definitions of the anisotropy ratio (e.g., Mauritsen and Svensson, 2007; Canut et al., 2015), which use all three wind components. However, the anisotropy ratio according to Eq. 3 can easily be compared to the values of the other definitions. In this case, $A = 1$ implies

145 isotropic turbulence. Values lower than 1 indicate day-time convection with a strong vertical turbulence component. Values exceeding 1 are caused by a dominating turbulence component in horizontal direction induced by wind shear.

For deriving the atmospheric stability regime, the gradient Richardson number Ri was determined with the formula used by Mauritsen and Svensson (2007), and applied by Conangla and Cuxart

150 (2006) for experimental and numerical LLJ studies:

$$Ri = \frac{\frac{g}{\theta} \frac{\partial \theta}{\partial z}}{(\frac{\partial u}{\partial z})^2 + (\frac{\partial v}{\partial z})^2} \quad (4)$$

For each flight, the mean gradient values of legs at 250 m and 200 m were used to calculate Ri , as these altitudes were probed during all four flights.

2.3 Low-Level Jet

155 The authors hypothesize that a Low-Level Jet (LLJ) was responsible for the high wind shear and turbulence in horizontal direction after sunset. Therefore, the phenomenon is shortly introduced. The LLJ consists of a maximum in the vertical profile of horizontal wind speed in the ABL, followed by a minimum of wind speed. This kind of wind profile does not follow the classical behaviour of wind speed increasing with altitude within the ABL until finally reaching the speed of the gradient or
160 geostrophic wind in the free troposphere, determined by the equilibrium of pressure gradient force, Coriolis force and centrifugal force.



The LLJ phenomenon has been observed and described for half a century (Blackadar, 1957). It is observed frequently, especially during night, with decoupling of the ABL from the ground during the development of a temperature inversion. Some climatologies observed a LLJ occurrence during
165 more than 30 to 60% of all nights (Song et al., 2005; Baas et al., 2009; Emeis, 2014; Lampert et al., 2015), with the exact value depending on location and strongly influenced by the different LLJ definitions. There are different criteria in the literature for identifying a wind profile as LLJ, e.g. taking into account the maximum wind speed, or a specific decrease of the wind speed above the altitude of the maximum wind speed (Banta, 2008). The LLJ is of importance for various atmospheric
170 processes. It has the capacity of horizontal transport of trace gases, aerosol, and water vapour during conditions of low near ground wind speed. Further, it creates wind shear and increase turbulence (e.g., Kallistratova et al., 2013).

3 Atmospheric situation

The day of 2 July 2011 was typical for a turbulently mixed ABL during the day with a decrease of
175 turbulence during the afternoon and evening hours. Solar irradiance measurements indicate a cloud-free day with values above 1000 W m^{-2} (Lothon et al., 2014, Fig. 6). The measurement site was influenced by a weak low pressure system above Portugal and a weak high pressure system North of Great Britain (Fig. 2). The ground wind speed was low ($1-3 \text{ m s}^{-1}$). The geostrophic wind speed should be low based on the low pressure gradient force, however, baroclinicity due to orographic
180 effects (sloping terrain, proximity of the Pyrene mountains) might enhance the real wind speed at higher altitudes. The wind direction was from North-West above Southern France, which turned to wind from North within the ABL. The ground wind direction turned from North to South-East during the transition period (Lothon et al., 2014). The maximum ABL height z_i observed during the AT with various measurement techniques (lidar, UHF, unmanned aircraft sounding) amounted
185 to 1200 m with another temperature inversion appearing at lower altitudes, indicating the residual layer (Lothon et al., 2014). A detailed overview of the general synoptic situation during BLLAST is provided in Lothon et al. (2014).

4 Results

4.1 ABL conditions

190 For describing the ABL conditions, vertical profiles of temperature, wind speed and wind direction obtained by the M²AV and the frequent radiosondes are analysed. The M²AV flight tracks represent the Northern part of the measurement area near site 1, while the frequent radiosondes represent the Southern part of the observation area near site 2 (Fig. 1).

The profiles of potential temperature up to altitudes of several 100 m during the four flights show



195 the evolution of the atmospheric stability during the AT (Fig. 3). They were all obtained during a
descent. During Flight 1 around 14:30 UTC (blue line), a potential temperature around 29°C was
observed. The profile indicates weakly unstable to weakly stable conditions. Note that the ascents
and descents of the M²AV are obtained with a horizontal aircraft speed of 22 m s⁻¹, and therefore lo-
cal temperature inhomogeneity created by varying surface conditions may influence the temperature
200 profiles. The potential temperature increased to values around 30°C for Flight 2 around 16:30 UTC
(red curve). The profile indicates weakly unstable to weakly stable conditions as well. The feature of
several values at the same altitude for the potential temperature, as e.g. at an altitude below 200 m,
are caused by a non-uniform decrease of flight altitude during the descent. During Flight 3 around
18:30 UTC (green curve), the potential temperature has decreased to values below 29°C. A weakly
205 stable stratification can be seen above 70 m altitude. Below, a strong temperature inversion is visible.
During Flight 4 around 20:30 UTC (black curve), the overall temperature has further decreased at all
altitudes. There is a weakly stable stratification with a mean potential temperature increase of 0.3 K
per 100 m between 100 and 400 m. Below 80 m, a strong temperature inversion of around 5 K per
100 m is present.

210 In the hourly radiosonde profiles, it can be seen that the temperature increased until 16:59 UTC (Fig.
4, green line). Then temperature decreased. The buildup of a ground based temperature inversion
below an altitude of 100 m is visible during the last two ascents and descents from 18:59 on (bold
magenta and cyan lines).

In Fig. 5, the wind profiles observed with the M²AV are shown for all flights. Note that the values
215 give an instantaneous profile, and not an average over 30 min as for the UHF wind profiler. The wind
speed near ground was small with values in the range of 1–5 m s⁻¹, in agreement with the ground
based wind measurements (Lothon et al., 2014). For Flight 1 and 2 (blue and red line), the wind speed
displays a maximum at an altitude around 80–90 m and then decreases again. The altitudes where the
turbulence measurements were performed (200–300 m) are above these wind speed maxima. Dur-
220 ing Flight 3 (green line), the wind increases slightly within the lowest 500 m, then decreases. At the
beginning of Flight 4 (magenta line), the wind conditions change. A strong wind speed exceeding
10 m s⁻¹ is recorded at an altitude of 40 m. In the next profiles of Flight 4, the wind speed increases
almost linearly with altitude (black lines) to a wind speed exceeding 5 m s⁻¹ above 100 m. The wind
speed decreases again above a local wind speed maximum at around 350 m altitude. Although the
225 wind profiles for Flight 4 are only available up to an altitude of 400 m, a broad wind speed maximum
of around 5–6 m s⁻¹ is obvious at an altitude interval around 150–370 m. Above, a decrease of the
wind speed to 4 m s⁻¹ can be seen for two of the profiles (solid and dashed black lines).

The radiosonde profiles of wind speed (Fig. 6) show low values of wind speed below 4 m s⁻¹, and
wind speed fluctuations with altitude similar to the M²AV wind profiles. During the last ascent and
230 descent at 19:57 UTC (bold cyan line), an LLJ profile was observed. The maximum wind speed of
around 4 m s⁻¹ was observed at 700–800 m altitude. The wind speed above the maximum decreased



more than 2 m s^{-1} until reaching a minimum at 1000 m altitude.

The wind direction measured with the M²AV was prevailing from North during the first three flights (Fig. 7). For Flight 4, a change in the wind direction can be observed. Therefore, all profiles
235 obtained during that flight are shown separately. The profile at 20:27 UTC (magenta line) still has a wind direction around North for the altitude interval around 50–120 m. Above and below, a wind direction of around 100° was observed. For the profiles observed later (21:06, 21:08 and 21:09 UTC), a prevailing wind direction around 100° was recorded.

The wind direction observed with the frequent radiosonde varied around North during the first ascents and descents of the afternoon (Fig. 8), in agreement with the M²AV observations. Around
240 18:59 UTC, a change in wind direction to 100° was recorded, which lasted throughout the last ascent and descent at 19:57. This is the same behaviour as observed with the M²AV, but with an earlier onset of the change of around 1 h.

Richardson numbers calculated for mean values of several horizontal M²AV legs have values around
245 and below the critical value of 0.25 for Flight 1 and 4, indicating an increase in TKE. During flight 2 and 3, Ri is exceeding values of 2, indicating a decrease of turbulence.

4.2 TKE and anisotropy development during afternoon transition

The turbulence properties were observed at altitudes between 150–300 m, corresponding to an altitude $z=0.17-0.25 z_i$ within the ABL height of 1200 m. The TKE values calculated for each flight
250 leg are displayed in Fig. 9 depending on altitude. The colour code indicates the flight where the data were obtained, each flight representing a specific time interval. Mean values averaged over all TKE values obtained at the same altitude for each flight are shown in the same figure but with bold symbols. There is a clear decrease of TKE between the observations during Flight 1 at 14:30 UTC (blue symbols) with mean values around $1.5 \text{ m}^2 \text{ s}^{-2}$ to the next observations of Flight 2 at 16:30
255 UTC (red symbols) with mean values around $0.6 \text{ m}^2 \text{ s}^{-2}$. During Flight 3 at 18:30 UTC, TKE has mean values of $0.03-0.04 \text{ m}^2 \text{ s}^{-2}$ (green symbols), corresponding to a very low wind speed and the building up of the nocturnal ABL and a temperature inversion near ground (Fig. 3). This was shortly before sunset at 19:42 UTC. During Flight 4 at 20:30 UTC, however, TKE increases again up to mean values around $0.25 \text{ m}^2 \text{ s}^{-2}$.

In Fig. 10, the temporal evolution of the anisotropy ratio is shown. For each leg, the mean value of A is displayed. For Flight 1 and 2 (blue and red symbols), many single values are below the horizontal line representing isotropic distribution of turbulence. However, the mean value is around 1 for both cases (bold symbols), indicating on the average local isotropic distribution of turbulence. The values of the anisotropy ratio range between 0.1 and 3. During Flight 3 around 18:30 UTC (green symbols),
265 directly before sunset, the mean anisotropy ratio is around 2, and the single values are between 0.5 and 6. During Flight 4, the anisotropy ratio has values between 2 and 40 with only one exception below 1. This lowest value of A was observed for the first horizontal leg of Flight 4, correspond-



ing to the time when the wind direction turned from North to East (magenta line in Fig. 7). As the anisotropy ratio changes from values around and below 1 to values exceeding 1, it can be deduced
270 that the main contribution to TKE is provided by the vertical wind component during Flight 1 and 2. Later, along with the development of a stable stratification, however, TKE is dominated by the horizontal component of the wind speed variance for Flight 3 at 18:30 UTC, which is even more pronounced for Flight 4 around 20:30 UTC.

The Richardson numbers indicate that turbulence is generated during the atmospheric conditions of
275 Flight 1 and 4, and suppressed during Flight 2 and 3. For Flight 1, this is caused by thermal generation of turbulence in a weakly unstable stratification. For Flight 4, the low Ri is created by dynamic generation of turbulence in stable conditions, i.e. a horizontal flow inducing turbulence in horizontal direction.

4.3 Low-Level Jet observations

280 After sunset, a nocturnal Low-Level Jet with a wind speed exceeding 8 m s^{-1} was observed with UHF radar at the more southerly located site 2 at an altitude of 100 to 400 m after 21:30 UTC (Fig. 11). Already from 16:00 UTC onwards, an increased wind speed was recorded up to an altitude of 800 m. The change in wind speed was accompanied with a change in wind direction from North to South-East, which is also evident in the radar data (not shown). The development of a LLJ profile
285 with linear increase of the wind speed up to a maximum at 800 m and a subsequent decrease in the wind speed above is in good agreement with the data of the frequent radiosonde for the launching place near site 2 at 19:57 UTC and near the balloon landing location, 9 km east of the launching location at 20:22 UTC (Fig. 6). This feature was not observed simultaneously at the more northerly location of site 1 (Fig. 12). However, around 800 m altitude, a wind speed maximum with wind speed
290 exceeding 6 m s^{-1} was observed around 23:00 UTC. Further, a LLJ appeared within the lowermost 400 m around midnight UTC and lasted until around 6:00 UTC (Fig. 13). Very likely, an LLJ affected the M²AV flight at 20:30 UTC.

5 Discussion

5.1 Turbulence properties

295 The TKE values observed with the M²AV are compatible with other TKE values obtained on that particular day with ground-based, balloon and airborne observations (Canut et al., 2015). In comparison with the time series of TKE for a similar day during BLLAST (Darbieu et al., 2015), the values of this case study are of similar magnitude for Flight 1 and Flight 2, but larger than modelled values at the corresponding altitude of $z=0.2 z_i$ with z_i the ABL height. For the time of Flight 3, the values
300 determined in this case study amount to about half of the values reported by Darbieu et al. (2015) both with observation and numerical modelling. However, the direct comparison of absolute TKE



values with other values in the literature is often difficult due to the non-unique definition of TKE and data treatment (e.g. over what time were the data averaged, was a high pass filtering technique applied or was a linear trend removal done for determining the wind speed variances, c.f. Banta et al. (2003)).

The change of TKE with altitude does not provide a clear tendency (Fig. 9). According to Banta (2008) a decrease of TKE with altitude is expected for an ABL where turbulence is created at the surface by thermal heating and then transported upwards. In contrast, when turbulence is induced by wind shear aloft, an increase of TKE with altitude is expected in the theory (Banta, 2008). In the Fig. 9, a large scatter of TKE values can be seen. This indicates that the single legs for deriving turbulence properties were too short and the terrain was too inhomogeneous to derive statistically representative values for individual flight legs (Lenschow et al., 1994). Note that the time for one flight leg is only about 45 s at the aircraft speed of 22 m s^{-1} , therefore providing only an instantaneous snapshot of the turbulence properties.

The change in anisotropy with higher values for the vertical component during the afternoon and higher values for the horizontal component after sunset is in accordance with other observations (Canut et al., 2015). The numerical simulations of Darbieu et al. (2015) determine an anisotropy ratio around 1 for the altitude $z=0.2 z_i$ and for the times of Flight 1 and 2, which agrees well with the mean observations of this case study. For the time of Flight 3, an anisotropy ratio around 2.5 is calculated, which is in agreement with the mean value of around 2 of the M^2AV measurements. The observations confirm the result of Darbieu et al. (2015) that the anisotropy ratio increases abruptly during the late afternoon, when the surface buoyancy flux amounts to zero before sunset.

5.2 Low-Level Jet as source of enhanced turbulence

In the climatology of Baas et al. (2009), a typical vertical profile and wind speed for LLJ were derived based on the inversion strength and the geostrophic wind forcing. The most pronounced LLJ profile, with the highest decrease in wind speed above the wind speed maximum, occurred for a geostrophic wind speed between 5 and 10 m s^{-1} 6 h after sunset. For these classes of LLJ events, the LLJ was most pronounced for a larger temperature inversion (temperature difference between 2 and 200 m exceeding 6 K). In this categorization of Baas et al. (2009), the case study very likely falls within those criteria. The wind speed at 3 km altitude revealed a value around 9 m s^{-1} at 2 UTC during that night. This high value might be a local orographic effect. No temperature profile is available at 2 UTC. However, the temperature profile obtained with the M^2AV at 20:30 UTC already shows an increase in the potential temperature of more than 4 K (Fig. 3). Due to the clear sky conditions, the temperature difference between ground and 200 m altitude very likely increased further during the night. Altogether, there were good conditions for the development of a pronounced LLJ.

The temporal development of the LLJ during the afternoon transition with increasing wind speed and a decrease of the maximum altitude with time has been described by e.g. Shapiro and Fedorovich



(2010). The dissipation of the LLJ after sunrise (at 4:24 UTC), when thermal turbulent mixing starts, is in agreement with most LLJ observations in the literature (e.g., Baas et al., 2009).

340 An LLJ increases the horizontal wind speed and is accompanied by vertical wind shear, and therefore can induce turbulence in a stably stratified atmosphere. This very likely explains the enhanced turbulence in horizontal direction measured in this case study. A generation of wind shear by interaction with friction forces induced by an inhomogeneous surface is not likely for two reasons: First, the turbulence measurements were performed at an altitude above 100 m, so a direct influence is not given. Second, a strong temperature inversion in the lowermost 70 m (Fig. 3) leads to a thermodynamic decoupling of the investigated altitudes from the atmosphere in direct contact with the surface. Conangla and Cuxart (2006) report values of the gradient Ri number below the critical value of 0.25 for several cases of LLJ below the LLJ core height. The profiles of wind direction obtained during Flight 4 (Fig. 7) indicate that the beginning of a LLJ event was captured with the observations. Only the first profile (magenta lines) shows a change in wind direction, while the other profiles during that flight (black lines) are similar to each other with a new wind direction of around 100°. The anisotropy ratio for the first leg is below 1 (Fig. 10), when the LLJ was still in the developing process. When the LLJ was fully developed, A exceeded 1 with enhanced horizontal wind speed variance induced by the wind shear of the LLJ.

355 There are different observations concerning the variance of the wind speed components during LLJ events: while the vertical profile of the variance of vertical wind speed σ_w^2 does not show enhanced values throughout the LLJ profile according to Kallistratova et al. (2013), and even a decrease of the horizontal wind speed variance σ_v^2 was reported for the LLJ altitude by Banta (2008), an increase in both the vertical and horizontal wind speed variance is described by Prabha et al. (2008). The observations presented in this case study reveal an inhomogeneous distribution of the LLJ. Although it was observed at all locations and with all techniques, the onset and intensity varied significantly within some km distance.

360

6 Conclusions

For a case study during the BLLAST field experiment on 2 July 2011, meteorological measurements with the M²AV captured the transition from a turbulently mixed ABL to a nocturnal stable ABL in Southern France. Vertical profiles of wind and potential temperature, as well as the turbulence properties TKE and anisotropy ratio were analysed. Additionally, data of UHF radar and frequent radiosonde are taken into account. The case study shows the development of TKE to smaller values with increasing atmospheric stability. The anisotropy ratio in the study starts to increase before sunset and continues increasing after sunset. In the case study it is shown that the increase in TKE and in the anisotropy ratio to a higher horizontal than vertical component took place simultaneously to the evolution of a LLJ. The LLJ was distributed inhomogeneously on a small scale of few km.

370



Acknowledgements. The authors would like to thank Andreas Scholtz and Thomas Krüger for piloting the M²AV during the BLLAST campaign. The BLLAST field experiment was made possible thanks to the contribution of several institutions and supports : INSU-CNRS (Institut National des Sciences de l'Univers, Centre national de la Recherche Scientifique, LEFE-IDAO program), Météo-France, Observatoire Midi-Pyrénées (University of Toulouse), EUFAR (EUropean Facility for Airborne Research) and COST ES0802 (European Cooperation in the field of Scientific and Technical). The field experiment would not have occurred without the contribution of all participating European and American research groups, which all have contributed in a significant amount (see supports). BLLAST field experiment was hosted by the instrumented site of Centre de Recherches Atmosphériques, Lannemezan, France (Observatoire Midi-Pyrénées, Laboratoire d'Aérodologie). The 60 m tower was partly supported by the POCTEFA/FLUXPYR European program. BLLAST data are managed by SEDOO, from Observatoire Midi-Pyrénées. The authors would like to thank Barbara Altstädter for critical proofreading the manuscript. The French ANR (Agence Nationale de la Recherche) is supporting the analysis of BLLAST dataset, and has funded this publication.



References

- Angevine, W. M., White, A. B., and Avery, S. K.: Boundary-layer depth and entrainment zone characterization with a boundary-layer profiler, *Bound.-Lay. Meteorol.*, 68, 375-385, 1994.
- Baas P., Bosveld F.C., Klein Baltink H., Holtslag A.A.M.: A Climatology of Nocturnal Low-Level Jets at
 390 Cabauw. *J. Appl. Meteor. Climatol.*, 48, 1627-1642, DOI: 10.1175/2009JAMC1965.1, 2009.
- Banta, R.M., Pichugina, Y.L., and Newsom, R.K.: Relationship between low-level jet properties and turbulence kinetic energy in the nocturnal stable boundary layer. *J. Atmos. Sci.*, 60, 2549-2555, 2003.
- Banta, R.M.: Stable-boundary-layer regimes from the perspective of the low-level jet. *Acta Geophysica*, 56, 1, 58-87, DOI: 10.2478/s11600-007-0049-8, 2008.
- 395 Blackadar, A.K.: Boundary layer wind maxima and their significance for the growth of nocturnal inversions. *Bull. Am. Met. Soc.*, 38, 283-290, 1957.
- Bonin, T., Chilson, P., Zielke, B., and Fedorovich, E.: Observations of the Early Evening Boundary-Layer Transition Using a Small Unmanned Aerial System, *Bound.-Lay. Meteorol.*, 146, 119-132, 2013.
- Busse, J., and Knupp, K.: Observed Characteristics of the Afternoon-Evening Boundary Layer Transition Based
 400 on Sodar and Surface Data, *J. App. Meteorol. Climatol.*, 51, 571-582, 2012.
- Canut, G., Couvreur, M., Lothon, M., Legain, D., Pigué, B., Lampert, A., and Moulin, E.: Turbulence measurements with a tethered balloon, submitted to *Atmos. Meas. Tech.*, 2015.
- Conangla, L., and J. Cuxart, J.: On the turbulence in the upper part of the low-level jet: An experimental and numerical study, *Bound.-Lay. Meteorol.*, 118, 379-400, 2006.
- 405 Darbieu, C., Lohou, F., Lothon, M., Vilà-Guerau de Arellano, J., Couvreur, F., Durand, P., Pino, D., Patton, E. G., Nilsson, E., Blay-Carreras, E., and Gioli, B.: Turbulence vertical structure of the boundary layer during the afternoon transition, *Atmos. Chem. Phys.*, 15, 10071-10086, doi:10.5194/acp-15-10071-2015, 2015.
- Emeis, S.: Wind speed and shear associated with low-level jets over Northern Germany. *Meteorologische Zeitschrift*, 23, 3, 295-304, DOI: 10.1127/0941-2948/2014/0551, 2014.
- 410 Gultepe, I., and Starr, D.O'C.: Dynamical Structure and Turbulence in Cirrus Clouds: Aircraft Observations during FIRE, *J. Atmos. Sci.*, 52, 23, 4159-4182, 1995.
- Jonassen, M.O., Tisler, P., Altstädter, B., Scholtz, A., Vihma, T., Lampert, A., König-Langlo, G., and Lüpkes, C.: Application of remotely piloted aircraft systems in observing the atmospheric boundary layer over Antarctic sea ice in winter, *Polar Research*, 34, 25651, <http://dx.doi.org/10.3402/polar.v34.25651>, 2015.
- 415 Kallistratova, M.A., Kouznetsov, R.D., Kramar, V.F., and Kuznetsov, D.D.: Profiles of Wind Speed Variances within Nocturnal Low-Level Jets Observed with a Sodar, *J. Atmos. Ocean. Technol.*, 30, 1970-1977, 2013.
- van den Kroonenberg A.C., Martin T., Buschmann M., Bange J., and Vörsmann, P.: Measuring the Wind Vector Using the Autonomous Mini Aerial Vehicle M²AV, *J. Atmos. Ocean. Technol.*, 25, 1969-1982, 2008.
- van den Kroonenberg, A., Martin, S., Beyrich, F., and Bange, J.: Spatially-Averaged Temperature Structure
 420 Parameter Over a Heterogeneous Surface Measured by an Unmanned Aerial Vehicle, *Bound.-Lay. Meteorol.*, 142, 55-77, 2012.
- Lampert, A., Bernalte Jimenez, B., Wulff, D., and Kenull, T.: One-year observations of the wind distribution and low-level jet occurrence at Braunschweig, North German Plain, accepted to *Wind Energy*, 2015.
- Legain, D., Bousquet, O., Douffet, T., Tzanos, D., Moulin, E., Barrie, J., and Renard, J.-B.: High frequency
 425 boundary layer profiling with reusable radiosondes, *Atmos. Meas. Tech.*, 6, 2195-2205, 2013.



- Lenschow, D.H., Mann, J., and Kristensen, L: How Long is Long Enough When Measuring Fluxes and Other Turbulence Statistics?, *J. Atmos. Ocean. Technol.*, 11, 661-673, 1994.
- Lothon, M., Lohou, F., Pino, D., Couvreux, F., Pardyjak, E. R., Reuder, J., Vilà-Guerau de Arellano, J., Durand, P., Hartogensis, O., Legain, D., Augustin, P., Gioli, B., Lenschow, D. H., Faloona, I., Yagüe, C., Alexander, D. C., Angevine, W. M., Bargain, E., Barrié, J., Bazile, E., Bezombes, Y., Blay-Carreras, E., van de Boer, A., Boichard, J. L., Bourdon, A., Butet, A., Campistron, B., de Coster, O., Cuxart, J., Dabas, A., Darbieu, C., Deboudt, K., Delbarre, H., Derrien, S., Flament, P., Fourmentin, M., Garai, A., Gibert, F., Graf, A., Groebner, J., Guichard, F., Jiménez, M. A., Jonassen, M., van den Kroonenberg, A., Magliulo, V., Martin, S., Martinez, D., Mastrorillo, L., Moene, A. F., Molinos, F., Moulin, E., Pietersen, H. P., Piguet, B., Pique, E., Romàn-Cascò, C., Rufin-Soler, C., Saïd, F., Sastre-Marugàn, M., Seity, Y., Steeneveld, G. J., Toscano, P., Traullé, O., Tzanos, D., Wacker, S., Wildmann, N., and Zaldei, A.: The BLLAST field experiment: Boundary-Layer Late Afternoon and Sunset Turbulence, *Atmos. Chem. Phys.*, 14, 10931-10960, doi:10.5194/acp-14-10931-2014, 2014.
- Lovejoy, S., Tuck, A.F., Hovde, S.J., and Schertzer, D.: Is isotropic turbulence relevant in the atmosphere?, *Geophys. Res. Lett.*, 34, L15802, doi:10.1029/2007GL029359, 2007.
- Martin, S., Bange, J., and Beyrich, F.: Meteorological profiling of the lower troposphere using the research UAV "M²AV Carolo", *Atmos. Meas. Tech.*, 4, 705-716, 2011.
- Martin, S., and Bange, J.: The Influence of Aircraft Speed Variations on Sensible Heat-Flux Measurements by Different Airborne Systems, *Bound.-Lay. Meteorol.*, 150, 153-166, 2014.
- Martin, S., Beyrich, F., and Bange, J.: Observing Entrainment Processes Using a Small Unmanned Aerial Vehicle: A Feasibility Study, *Bound.-Lay. Meteorol.*, 150, 449-467, doi:10.1007/s10546-013-9880-4, 2014.
- Mauritsen, T., and Svensson, G.: Observations of Stably Stratified Shear-Driven Atmospheric Turbulence at Low and High Richardson Numbers, *J. Atmos. Sci.*, 64, 645-655, 2007.
- Meischner, P., Baumann, R., Höller, H., and Jank, T.: Eddy Dissipation Rates in Thunderstorms Estimated by Doppler Radar in Relation to Aircraft In Situ Measurements, *J. Atmos. Ocean. Technol.*, 18, 1609-1627, 2001.
- Nadeau, D. F., Pardyjak, E. R., Higgins, C. W., Fernando, H. J. S., and Parlange, M. B.: A simple model for the afternoon and early evening decay of convective turbulence over different land surfaces, *Bound.-Lay. Meteorol.*, 141, 301-324, 2011.
- Paluch, I.R., and Baumgardner, D.G.: Entrainment and Fine-Scale Mixing in a Continental Convective Cloud, *J. Atmos. Sci.*, 46, 2, 261-278, 1989.
- Prabha, T.V., Leclerc, M.Y., Karipot, A., Hollinger, D.Y., and Mursch-Radlgruber, E.: Influence of Nocturnal Low-level Jets on Eddy-covariance Fluxes over a Tall Forest Canopy, *Bound.-Lay. Meteorol.*, 126, 219-236, 2008.
- Shapiro A., and Fedorovich E.: Analytical description of a nocturnal low-level jet, *Q.J.R. Meteorol. Soc.*, 136, 1255-1262, DOI: 10.1002/qj.628, 2010.
- Song, J., Liao, K., Coulter, R.L. and Lesht, B.M.: Climatology of the low-level jet at the southern Great Plains Atmospheric Boundary Layer Experiment Site. *J. Appl. Meteor.*, 44, 1593-1606, 2005.
- Spieß, T., Bange, J., Buschmann, M., and Vörsmann, P.: First application of the meteorological Mini-UAV 'M²AV', *Meteorologische Zeitschrift*, 16, 2, 159-169, 2007.



Stickney, T.M., Shedlov, M.W., and Thompson, D.I.: Goodrich Total Temperature Sensors, Technical Report, 5755, C, 32 pp. <http://www.faam.ac.uk/index.php/faam-documents/science-instruments/47-rosemount-report-5755/file>, 1994.

Stull, R.B.: An Introduction to Boundary Layer Meteorology, Kluwer Academic Publishers, Reprint 1991, 666
470 pp., 1988.

Thebaud, L.: An atmospheric turbulent velocity spectrum for three dimensions, *J. Geophys. Res.*, 109, D10109, doi:10.1029/2002JD003173, 2004.

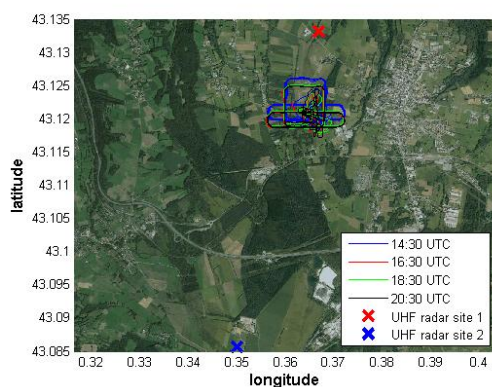


Figure 1. Geographic overview of the data obtained during the BLLAST field experiment: flight tracks of the M²AV (lines) and locations of the two UHF wind profiler (cross symbols). The frequent radiosonde was launched close to site 2, and landed depending on the wind direction and speed.

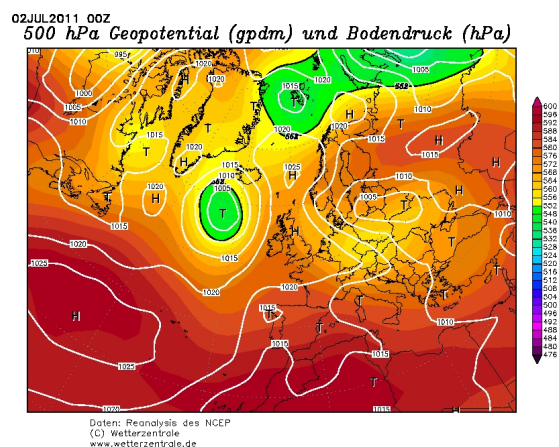


Figure 2. Synoptic situation on 2 July 2011, NCEP reanalysis data, obtained from the archive of www.wetterzentrale.de

Table 1. Takeoff and landing time for each flight of the M²AV on 2 July 2011.

Flight	takeoff [UTC]	landing [UTC]
1	14:31	15:14
2	16:36	16:59
3	18:23	19:04
4	20:26	21:10

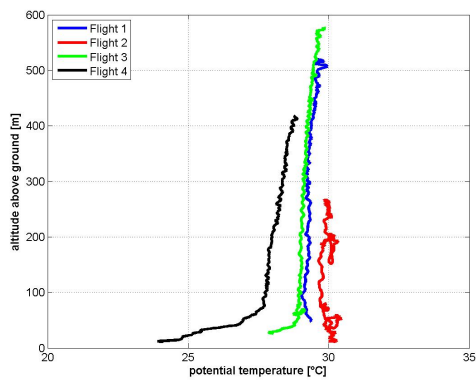


Figure 3. Profiles of potential temperature obtained with the M²AV near site 1.

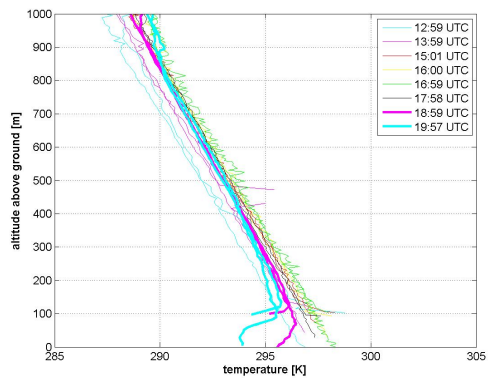


Figure 4. Profiles of temperature obtained with the frequent radiosonde near site 2.

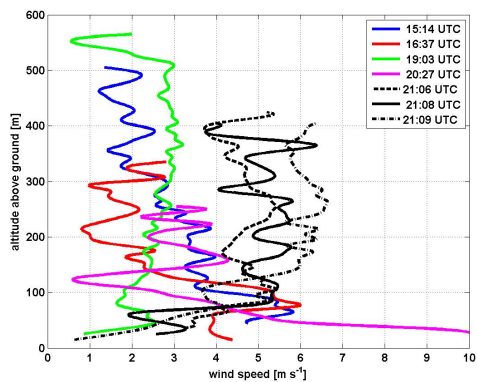


Figure 5. Profiles of wind speed in $[m s^{-1}]$ obtained with the M^2AV near site 1.

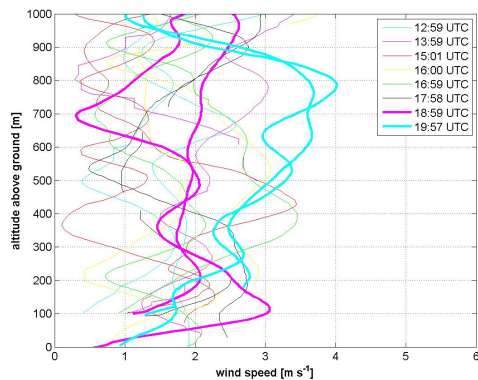


Figure 6. Profiles of wind speed in $[m s^{-1}]$ obtained with the frequent radiosonde near site 2.

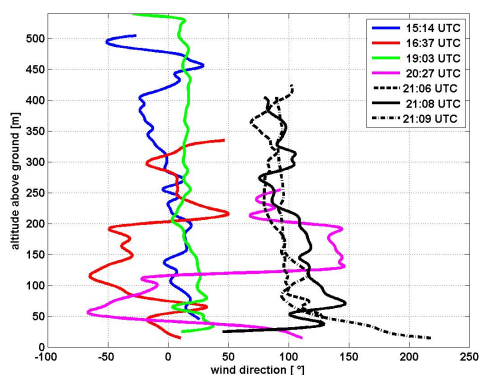


Figure 7. Profiles of wind direction in $^{\circ}$ obtained with the M^2AV near site 1. For avoiding artificial jumps in the profiles when passing North (0 and 360°), the wind direction in the sector between West (270°) and North (360°) is displayed as negative wind direction.

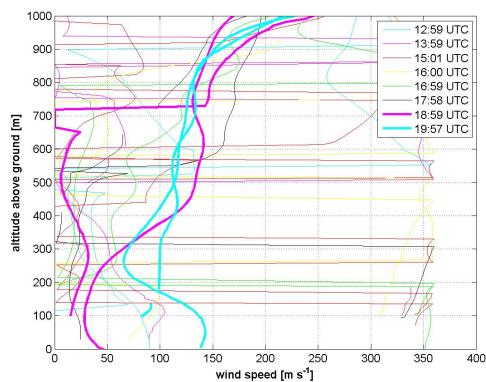


Figure 8. Profiles of wind direction in $^{\circ}$ obtained with the frequent radiosonde near site 2. Note that jumps between 0 and 360° indicate that the wind direction is varying slightly around North.

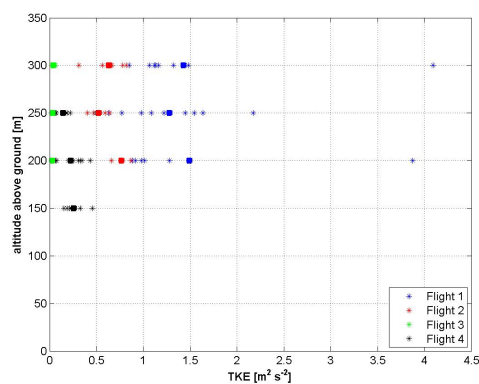


Figure 9. TKE calculated for each flight leg of around 1 km length. The values were obtained by high pass filtering the data with a frequency of 0.01 Hz. The mean values averaged over all flight legs at the same altitude for each flight are indicated with larger point size.

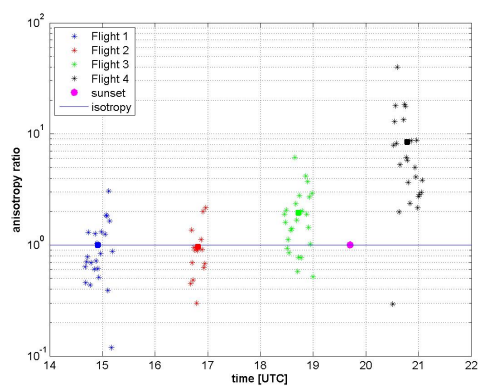


Figure 10. Time series of the anisotropy parameter obtained with the M^2 AV. The horizontal line indicates isotropy according to the definition. The mean values of the anisotropy parameter for each flight are given as thick dots. The magenta dot indicates the time of sunset.

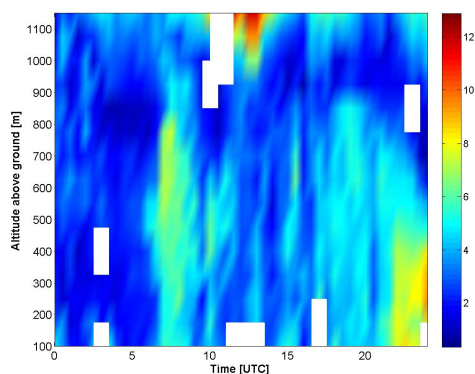


Figure 11. Temporal evolution of the wind speed in $[m s^{-1}]$ observed by UHF radar at site 2 on 2 July 2011. The data are averaged over 30 min and have a vertical resolution of 75 m. Erroneous values and data gaps are indicated in white. A LLJ is apparent in the lowest 300 m after 21:30 UTC.

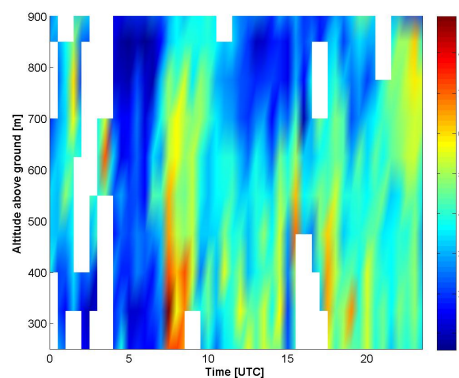


Figure 12. Temporal evolution of the wind speed in $[m s^{-1}]$ observed by UHF radar at site 1 on 2 July 2011. The data are averaged over 30 min and have a vertical resolution of 75 m. Erroneous values and data gaps are indicated in white.

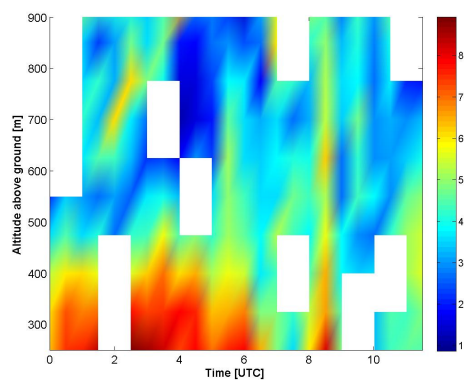


Figure 13. Temporal evolution of the wind speed in m s^{-1} observed by UHF radar at site 1 during the following day on 3 July 2011. The data are averaged over 30 min and have a vertical resolution of 75 m. Erroneous values and data gaps are indicated in white. A LLJ was recorded from midnight to around 6 UTC up to 400 m altitude.